

Use of a Mylar filter to eliminate vacuum ultraviolet pulse pileup in low-energy x-ray measurements

Cite as: Rev. Sci. Instrum. **93**, 093531 (2022); <https://doi.org/10.1063/5.0101712>

Submitted: 02 June 2022 • Accepted: 15 August 2022 • Published Online: 30 September 2022

 C. A. Galea,  C. P. S. Swanson,  S. A. Cohen, et al.





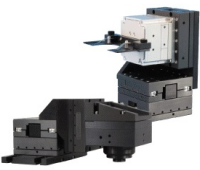
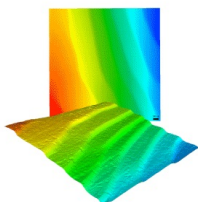
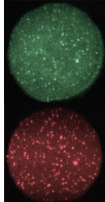
View Online



Export Citation



CrossMark

	<p>Nanopositioning Systems</p> 	<p>Modular Motion Control</p> 	<p>AFM and NSOM Instruments</p> 	<p>Single Molecule Microscopes</p> 
---	--	--	---	--

Use of a Mylar filter to eliminate vacuum ultraviolet pulse pileup in low-energy x-ray measurements

Cite as: Rev. Sci. Instrum. 93, 093531 (2022); doi: 10.1063/5.0101712

Submitted: 2 June 2022 • Accepted: 15 August 2022 •

Published Online: 30 September 2022



View Online



Export Citation



CrossMark

C. A. Galea,^{1,a)} C. P. S. Swanson,² S. A. Cohen,² and S. J. Thomas¹

AFFILIATIONS

¹Princeton Fusion Systems, Plainsboro, New Jersey 08536, USA

²Princeton Plasma Physics Laboratory, Princeton University, Princeton, New Jersey 08543, USA

Note: This paper is part of the Special Topic on Proceedings of the 24th Topical Conference on High-Temperature Plasma Diagnostics.

^{a)}Author to whom correspondence should be addressed: cgalea@psatellite.com

ABSTRACT

We describe a method to reduce vacuum ultraviolet (VUV) pulse pileup (PPU) in x-ray pulse-height Silicon Drift Detector (SDD) signals. An Amptek FAST SDD, with C1 (Si_3N_4) window, measures bremsstrahlung emitted from PFRC-2 plasma to extract the electron temperature (T_e) and density (n_e). The C1 window has low transmissivity for photons with energy below 200 eV though will transmit some VUV and soft x-ray photons, which PFRC-2 plasmas abundantly emit. Multi-VUV-photon PPU contaminates the interpretation of x rays with energy > 100 eV, particularly in a low-energy exponential tail. The predicted low transmissivity of $\sim 1 \mu\text{m}$ thick Mylar [polyethylene terephthalate (PET)] to photons of energy < 100 eV led to the selection of Mylar as the candidate filter to reduce VUV PPU. Experiments were conducted on an x-ray tube with a graphite target and on a quasi-Maxwellian tenuous plasma ($n_e \sim 10^9 \text{ cm}^{-3}$) with effective temperatures reaching 1500 eV. A Mylar filter thickness of 850 nm is consistent with the results. The Mylar-filter-equipped SDD was then used on the PFRC-2 plasma, showing a substantial reduction in the low-energy x-ray signal, supporting our hypothesis of the importance of VUV PPU. We describe the modeling and experiments performed to characterize the effect of the Mylar filter on SDD measurements.

Published under an exclusive license by AIP Publishing. <https://doi.org/10.1063/5.0101712>

I. INTRODUCTION

The Princeton Field-Reversed Configuration-2 (PFRC-2) is an FRC heating and confinement experiment.¹ The FRC plasma is formed and heated by odd-parity rotating magnetic fields (RMF_o). The PFRC-2 plasma emits x rays via bremsstrahlung and line emission. Bremsstrahlung radiation is of interest in order to measure electron energy distribution functions (EEDFs),² from which electron number density n_e and temperature T_e can be extracted. Figure 1 shows schematics of the PFRC-2 experiment where an FRC is present (bottom) and without the FRC (top), which occurs in the absence of RMF_o . Two Silicon Drift Detector (SDD) x-ray pulse-height detectors in the center cell measure the x-ray emission above 150 eV from two viewing chords. A microwave interferometer is used for electron density measurements of the bulk plasma. The x-ray lines-of-sight (LOSs) are indicated in the figure.

The x-ray detectors in our experiments, Amptek FAST SDD X-123, perform x-ray pulse-height energy analysis.³ As the x-ray count rate increases, which frequently occurs during RMF_o plasma heating, there is increased probability of two or more x rays arriving at the detector within the pileup resolving time and thus being registered as one x ray with energy greater than that of a single incident x ray and less than or equal to the energy sum of the incident x rays. This phenomenon is referred to as pulse pileup (PPU). PPU presents an issue to x-ray measurements of high-count-rate sources since it corrupts the x-ray spectra, resulting in erroneous measurements of properties of interest. For PFRC-2 RMF_o plasma, various spectra were found to be distorted by PPU, inferred from changes in spectra shape with changes in x-ray flux. The light-tight C1 window by Amptek,⁴ composed of a mesh-supported aluminum-coated silicon-nitride (Si_3N_4) film installed with the SDD, has a region of higher transmissivity in the vacuum ultraviolet (VUV) region, and,

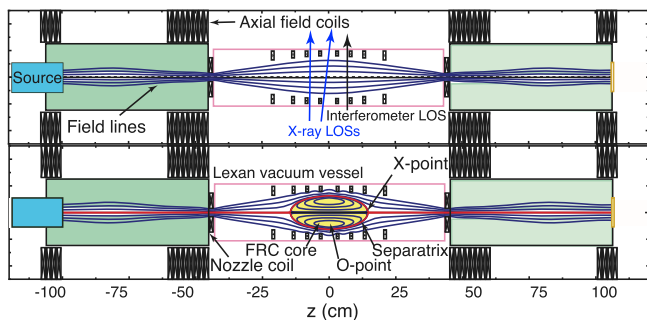


FIG. 1. PFRC-2 schematics: (top) without an FRC present; (bottom) with an FRC plasma. The pre-FRC seed target plasma is contained within the envelope of the field lines depicted over the full axial extent. The two SDDs along with their lines of sight (indicated as “X-ray LOSs” in the figure) are shown in the top half of the figure.

hence, was unable to prevent this PPU. The potential for PPU to be generated by this photon energy range in the PFRC-2 was the impetus to investigate the Mylar filter.

In this paper, we investigate the use of a Mylar filter to eliminate VUV PPU in SDD signals. Section II. describes the pulse-pileup issue in PFRC-2 x-ray measurements and introduces the Mylar filter along with its properties as a potential solution to resolve VUV PPU. The details of how the Mylar filter fits into the x-ray data analysis along with the calibration of x-ray spectra with the Mylar filter are described in Sec. III. Section IV. describes results enabled by the implementation of the Mylar filter, including elimination of pulse pileup in RMF_o plasmas and the ability to measure bremsstrahlung with even higher power RMF_o.

II. MYLAR FILTER WINDOW FOR ELIMINATING PULSE PILEUP

Under certain conditions, the x-ray spectra measured from the PFRC-2 exhibit behavior that we attribute to PPU. An example can be seen in Fig. 2, which shows x-ray spectra for various apertures that limit the x-ray flux into the SDD because of their different aperture

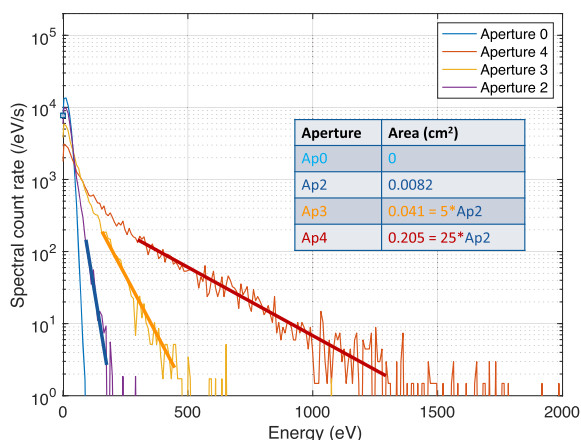


FIG. 2. Comparison between various aperture sizes for x-ray spectra. Aperture areas are listed to the right of the spectra. $B(0,0) = 228$ G, $P_{\text{RMF}} = 31$ kW, $f_{\text{RMF}} = 6.02$ MHz, and hydrogen fill pressure = 0.39 mTorr.

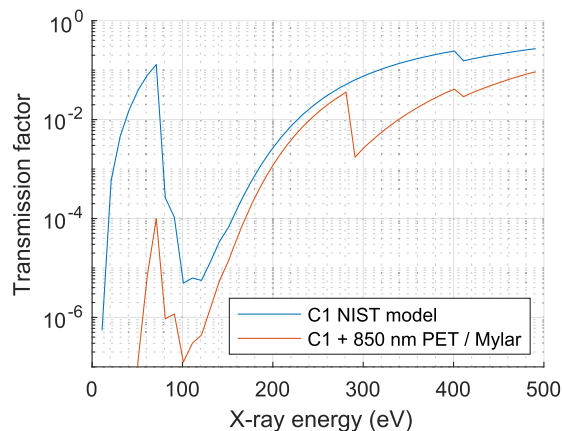


FIG. 3. Transmissivity vs photon energy for the Amptek C1 window and the C1 window with added 850 nm thick PET/Mylar filter.⁵ At low photon energy, the C1 window is transmissive, reaching 10% at 70 eV.

areas. If there were no PPU, increasing the aperture area would result in the same spectral distribution, albeit with an augmented spectral count rate. However, we observe that increasing the aperture area causes the spectrum to extend to higher energies, which is indicative of PPU. The “noise” spectrum region (10–200 eV) correspondingly decreases with increasing aperture size, also consistent with PPU. Pileup would alter the x-ray spectrum’s slope, which thus affects the measurement of electron temperature T_e .

Figure 3 shows the transmission curve for the Amptek C1 window installed with the SDD and that for the C1 window plus 850 nm PET/Mylar filter. In our analyses, Mylar is assumed to be pure polyethylene terephthalate (PET) with unit formula $C_{10}H_8O_4$. The C1 window has an aluminum coating with Al L-edge at 70 eV, which results in a transmissive energy range with centroid at 61 eV.

In the energy range $E < 200$ eV, the values of the x-ray transmissivity are only approximately known.⁵ Because of this, it is not possible to say definitively that bremsstrahlung from Maxwellian electrons produces enough x-ray flux around 61 eV to cause the inferred pileup. Taking the NIST model at face value, the amount of pileup inferred is consistent with bremsstrahlung from $n_e \sim 5 \times 10^{13}$ /cc, $T_e \sim 60$ eV.



FIG. 4. Photograph of the Mylar window. The nominal thickness from the manufacturer is 1 μm . However, 850 nm thickness is found to better agree with the measurement. This discrepancy may be due to either the thickness or the uncertainty in the x-ray attenuation factors at low energy.⁵

A removable Mylar window, shown in Fig. 4, was installed in front of an SDD to significantly reduce pulse pileup. The Mylar attenuates the photons in the 60 eV region by a factor of 1000 while transmitting higher energy photons, those of interest for x-ray measurements, such as of T_e . The implementation of the Mylar filter requires only a hoop on a Wilson seal, the ease of which makes the Mylar filter a practical approach.

III. DATA ANALYSIS AND CALIBRATION FOR THE MYLAR FILTER

Figure 5 illustrates the x-ray path from plasma emission to detector measurement and where the Mylar filter fits into the x-ray data analysis. Analyzing the effect of the Mylar filter on the spectra requires knowledge of the matrices for each step in the figure.² From left to right: The PFRC-2 plasma with a given electron energy distribution function (EEDF) emits x rays with a corresponding x-ray energy distribution function (XEDF); the bremsstrahlung transformation matrix M_{Brems} converts the EEDF to XEDF. The X rays then pass through the Mylar filter, then through the Amptek C1 window, and finally are recorded by the SDD. The corresponding matrices for these transmission steps are the Mylar transmission matrix M_{Mylar} , the C1 window transmission matrix M_{Win} , and the detector resolution matrix M_{res} . The bremsstrahlung, window, and resolution matrices are described in Ref. 2. A first approximation comparison multiplies the XEDF with no Mylar filter by M_{Mylar} , while a more detailed comparison includes convolution with the detector response M_{res} .

Calibration of the effects of the Mylar filter were conducted in an x-ray tube with a graphite target. In the x-ray tube, thermionically emitted electrons are accelerated to 5 keV by a DC voltage source. Figure 6 compares the measured x-ray spectra with no Mylar filter to that measured with the Mylar filter and additionally plots the no-filter measurement multiplied by the NIST transmission model⁵ for 850 nm of Mylar. There is good agreement between the data taken with the Mylar filter and the no-filter data corrected by the transmission model for energies above 600 eV. The Gaussian peaks at 277, 392, and 525 eV are narrow lines corresponding to the carbon, nitrogen, and oxygen K- α lines, respectively, blurred by the detector's (mostly Gaussian) response. The peak at 1.7 keV is due to Si, most likely fluorescence of the C1 window. Figure 7 shows the ratio of with-filter to no-filter measurements, the NIST transmission model for 850 nm, and the NIST model convolved by the SDD response, for

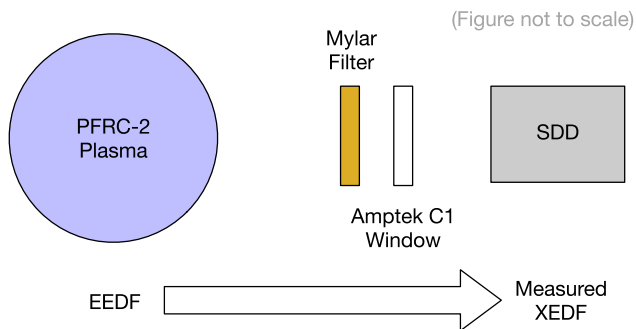


FIG. 5. Diagram showing the path from plasma EEDF to the XEDF measured by the SDD.

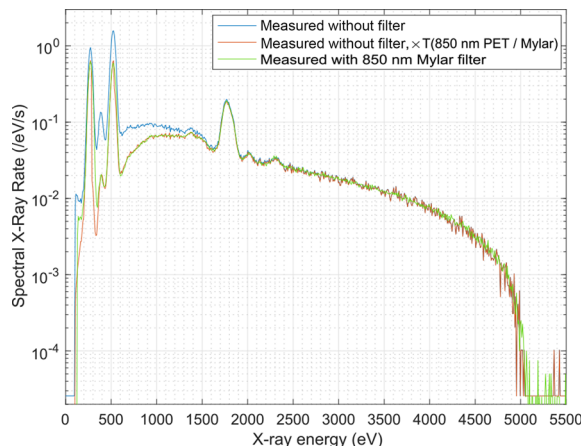


FIG. 6. Calibration data from the x-ray tube. Plotted in this figure are the measured x-ray spectra with no filter and with the Mylar filter, and the no-filter measurement multiplied by the NIST transmission model⁵ for 850 nm thick Mylar. Good agreement is seen between the latter two curves.

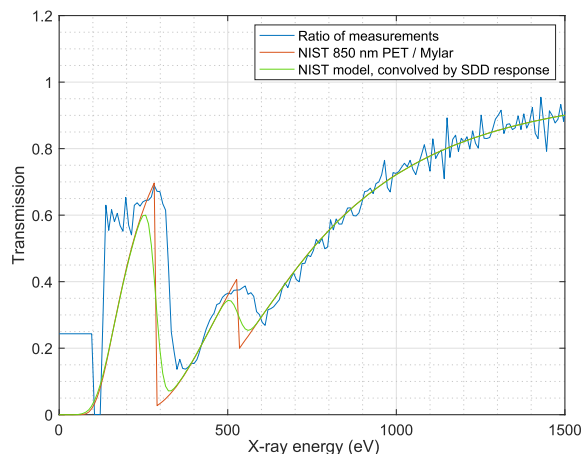


FIG. 7. Transmission calibration data from the x-ray tube zoomed in to energies below 1500 eV. Plotted in the figure are the ratio of with-filter to no-filter measurements, the NIST transmission model⁵ for 850 nm Mylar, and the NIST model convolved by the SDD response. Including the effect of the SDD response blurs the sharp edges of the NIST model, bringing it closer in behavior to the measured data.

energies less than 1500 eV. The sharp edges of the NIST model are blurred by the SDD response, bringing the curve closer in behavior to the measurement data. The calibration results show that 850 nm of Mylar is the best fit with transmission data.

IV. RESULTS ENABLED BY THE MYLAR FILTER

In this section, we describe various x-ray measurements made with the Mylar filter. The first results described are for a quasi-Maxwellian tenuous plasma ($n_e \sim 10^9 \text{ cm}^{-3}$), known to contain a hot minority component reaching $T_e \sim 1500 \text{ eV}$. X-ray spectra from this plasma, also called the PFRC-2 “seed” plasma, are shown in Fig. 8. Measurements without the Mylar filter were compared to measurements with the Mylar filter divided by the Mylar transmissivity; good

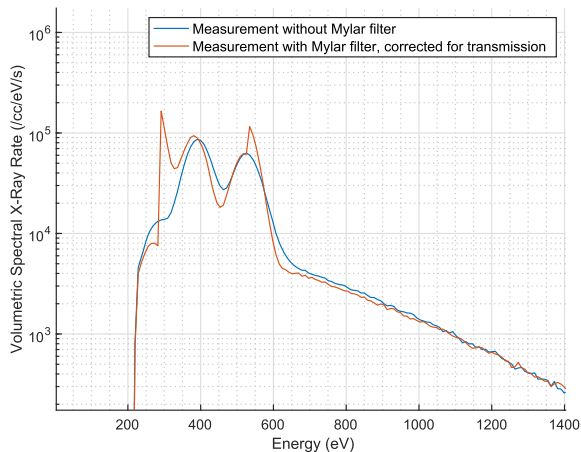


FIG. 8. Seed plasma spectra taken without Mylar and with Mylar, where the latter was divided by the Mylar transmissivity. RF (27 MHz) power = 205 W, $B(0,0) = 126$ G, helium fill pressure = 0.36 mTorr. The sharp jumps in the corrected data are artifacts of the analysis.

agreement is found. Sharp jumps in the “corrected” data are artifacts of analysis, as the measurement is subject to the broad response of the SDD while the transmissivity correction factor has discontinuities at the electron shell edge energies associated with the carbon and oxygen atoms contained in the Mylar. The broad peaks of the spectral lines are found to agree.

We now consider the impact of the Mylar filter on PFRC-2 RMF plasmas. In Fig. 9, x-ray spectra are recorded from PFRC-2 RMF plasma in a high-UV-flux condition. The spectrum measured with no Mylar filter shows a broad range of x-ray energies, heavily distorted by pileup, while the *same* spectrum measured with the Mylar filter shows a drastically different behavior—the x-ray spectrum behind the pileup is revealed. The Mylar filter window successfully eliminates the pulse pileup. This spectrum is included

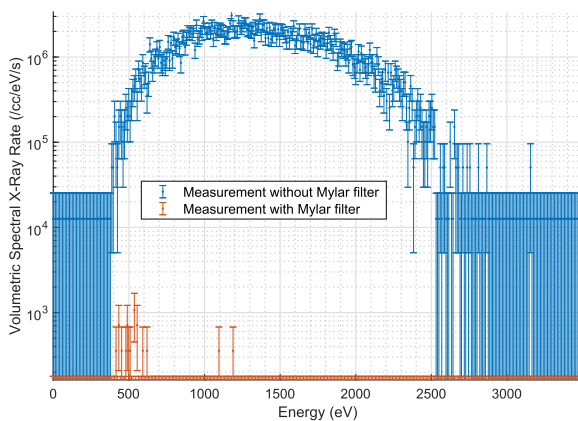


FIG. 9. Spectra recorded from PFRC-2 RMF plasma in high-UV-flux condition. The blue data were recorded without the Mylar filter, showing a spectrum obscured by pileup. The red data were recorded with the Mylar filter, revealing the x-ray spectrum behind the pileup. $B(0,0) = 223$ G, helium fill pressure = 0.35 mTorr, $P_{\text{RMF}} = 60$ kW, $f_{\text{RMF}} = 4.3$ MHz.

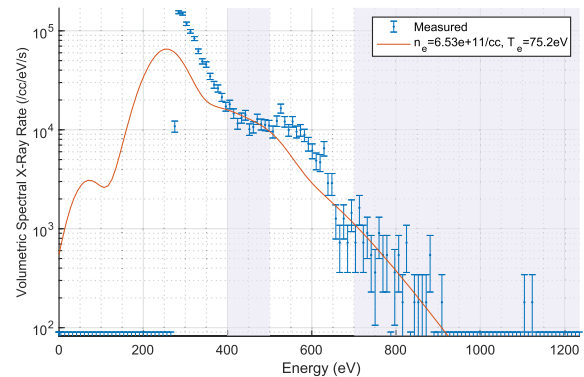


FIG. 10. X-ray spectrum for 70 kW RMF case. The SDD slow threshold was set to eliminate counts below ~ 250 eV. $P_{\text{RMF}} = 70$ kW, $B = 230$ G, pressure = 0.482 mTorr, $f_{\text{RMF}} = 4.3$ MHz. Hydrogen fill gas.

for illustration purposes; the plasma was formed using helium gas fill.

The Mylar filter’s ability to eliminate pulse pileup enables measurements of electron energies in the PFRC-2 RMF plasma, undistorted by VUV PPU. Maxwellian fits were performed on the x-ray spectra to obtain electron number density and temperature. Two cases are now presented. Figure 10 shows an x-ray spectrum from hydrogen plasma in the PFRC-2 with 70 kW RMF. The electron density (top part of Fig. 11) decays from 4×10^{12} to 1.2×10^{12} cm^{-3} . (Density was extracted from the line-averaged interferometer measurements and assumed an 8 cm plasma radius.) Often, when n_e decays in an RMF_o-heated plasma, the x-ray count rate (bottom part of Fig. 11) increases. The x-ray spectrum shown is attributable to bremsstrahlung and an oxygen K- α line at 525 eV. The fit in Fig. 10 is valid above 400 eV. Extrapolated down to 0 eV, the maximum inferred Maxwellian fit density during the pulse (corrected for pressure drop) would be 6.5×10^{11} cm^{-3} .

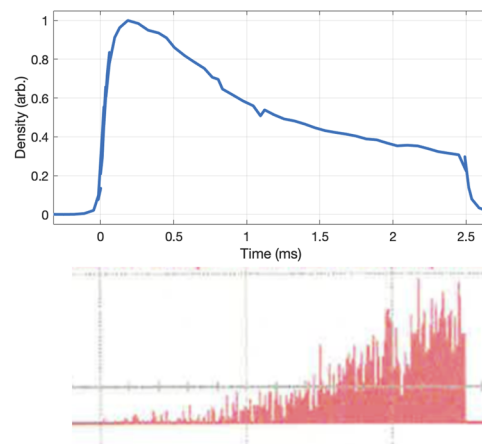


FIG. 11. Interferometer trace of electron number density digitized using WebPlotDigitizer⁶ (top) and x-ray pulses vs time with 1 ms/division (bottom) for 70 kW RMF case, accumulated from ~ 300 2.5 ms-duration pulses. $P_{\text{RMF}} = 70$ kW, $f_{\text{RMF}} = 4.3$ MHz, RMF duty factor = 0.04, $B(0,0) = 230$ G, hydrogen fill pressure = 0.482 mTorr.

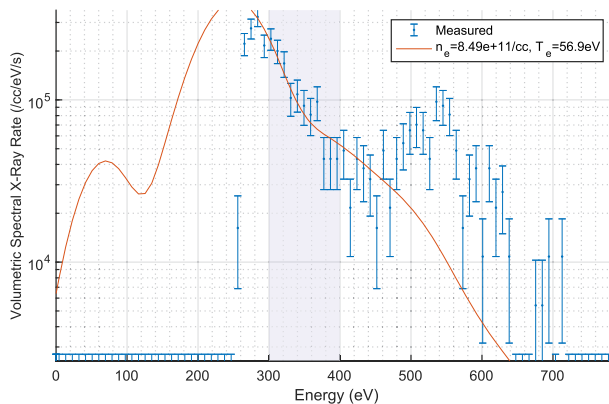


FIG. 12. X-ray spectrum for 100 kW RMF case. The SDD slow threshold was set to eliminate counts below ~ 250 eV. $P_{\text{RMF}} = 100$ kW, $B = 185$ G, pressure = 1.5 mTorr, $f_{\text{RMF}} = 4.3$ MHz. Hydrogen fill gas.

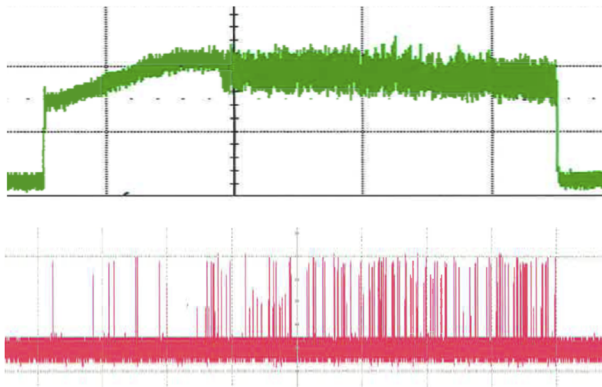


FIG. 13. Top: Interferometer trace of n_e vs time, 40 ms-duration RMF. Bottom: X-ray pulse arrival time vs time. $P_{\text{RMF}} = 100$ kW, $f_{\text{RMF}} = 4.3$ MHz, $B(0,0) = 185$ G, pressure = 1.5 mTorr.

Finally, we consider x rays from higher power, 100 kW, RMF_o-heated plasmas, observed by an SDD equipped with a Mylar filter. (The gas fill pressure was high, to increase the UV flux and lower T_e , in order to test the Mylar filter under extreme conditions.) Fig. 12 shows the x-ray spectrum from a single RMF_o pulse along with a Maxwellian fit. At this power level, the count rate has reached 2×10^4 s. The oxygen K- α line is visible at 525 eV. The broad energy spread around the oxygen K- α line led to the choice of fit range before this region: 300–400 eV. X-ray Maxwellian fit parameters are $n_e = 8.5 \times 10^{11} \text{ cm}^{-3}$, $T_e = 57$ eV. Figure 13 shows the interferometer electron density time trace and x-ray time histogram for the RMF pulse. The full pulse is 40 ms. The maximum n_e is $2.7 \times 10^{12} \text{ cm}^{-3}$. X-ray measurements are not contaminated by PPU in this high-count-rate regime, thanks to the Mylar filter.

V. CONCLUSIONS

To test its ability to ameliorate UV-emission-generated pulse-pileup effects in pulse-height x-ray detectors, an 850 nm Mylar filter was fabricated, calibrated, and operated on the PFRC-2 device. X-ray measurements were made under high-UV-flux conditions.

The Mylar filter permits x-ray spectrum measurement in regimes previously distorted by pulse pileup caused by low-energy photons. The filter is an accessible solution, requiring only a hoop on a Wilson seal for implementation. The measured XEDFs in 50–100 kW discharges are described by Maxwellian extrapolations approaching bulk density and Maxwellian fit temperatures of 50–75 eV.

ACKNOWLEDGMENTS

This work was supported by the U.S. Department of Energy under Contract No. DE-AC02-09CH11466. The United States Government retains a nonexclusive, paid-up, irrevocable, worldwide license to publish or reproduce the published form of this manuscript, or allow others to do so, for United States Government purposes.

This work was also supported by ARPA-E Award No. DE-AR0001099 (Princeton Fusion Systems) and the Princeton Program in Plasma Science and Technology, Princeton University. We are grateful to M. Paluszek for support and to B. Berlinger and C. Brunkhorst for excellent technical work.

AUTHOR DECLARATIONS

Conflict of Interest

The authors have no conflicts to disclose.

Author Contributions

C. A. Galea: Data curation (equal); Formal analysis (equal); Writing – original draft (lead); Writing – review & editing (equal). **C. P. S. Swanson:** Conceptualization (equal); Data curation (lead); Formal analysis (equal); Writing – review & editing (equal). **S. A. Cohen:** Conceptualization (equal); Investigation (equal); Writing – review & editing (equal). **S. J. Thomas:** Data curation (equal); Formal analysis (supporting); Funding acquisition (equal); Writing – original draft (supporting); Writing – review & editing (equal).

DATA AVAILABILITY

The data that support the findings of this study are available from the corresponding author upon reasonable request.

REFERENCES

- S. Cohen, C. Brunkhorst, A. Glasser, A. Landsman, and D. Welch, “RF plasma heating in the PFRC-2 device: Motivation, goals, and methods,” *AIP Conf.* **1406**, 273–276 (2011).
- C. Swanson, P. Jandovitz, and S. A. Cohen, “Using Poisson-regularized inversion of Bremsstrahlung emission to extract full electron energy distribution functions from x-ray pulse-height detector data,” *AIP Adv.* **8**, 025222 (2018).
- T. Pantazis, J. Pantazis, A. Huber, and R. Redus, “The historical development of the thermoelectrically cooled X-ray detector and its impact on the portable and hand-held XRF industries,” *X-Ray Spectrom.* **39**, 90 (2010).
- See <https://www.amptek.com/products/x-ray-detectors/fastddd-x-ray-detectors-for-xrf-eds/c-series-low-energy-x-ray-windows> for Patented C-Series Low Energy X-Ray Windows; accessed May 22, 2022.
- C. T. Chantler, K. Olsen, R. A. Dragoset, J. Chang, A. R. Kishore, S. A. Kotochigova, and D. S. Zucker, see <http://physics.nist.gov/ffast> for X-Ray Form Factor, Attenuation and Scattering Tables (version 2.1), 2005; accessed May 22, 2022.
- A. Rohatgi, see <https://automeris.io/WebPlotDigitizer> for WebPlotDigitizer, 2020; accessed August 8, 2022.